Micromachined *W*-Band Filters

Stephen V. Robertson, *Student Member, IEEE*, Linda P. B. Katehi, *Fellow, IEEE*, Gabriel M. Rebeiz, *Senior Member, IEEE*

Abstract— **Results are presented for high performance planar W-band filters based on silicon micromachining techniques common in microsensor fabrication. Two types of micromachined planar transmission lines are studied: microshield line and shielded membrane microstrip (SMM) line. In both of these structures, the conducting lines are suspended on thin dielectric membranes. These transmission lines are essentially "floating" in air, possess negligible levels of dielectric loss, and do not suffer from the parasitic effects of radiation and dispersion. A 90 GHz low pass filter and several 95 GHz bandpass filters are tested and display excellent performance which cannot be achieved with traditional substrate supported circuits in CPW or microstrip configurations. A full-wave finite-difference time-domain (FDTD) technique verifies the measured performance of the W-band circuits and provides a basis for comparison between the performances of membrane supported circuits and equivalent substrate supported circuits.**

I. Introduction

MILLIMETER wave integrated circuits require low-loss, low-dispersion, planar transmission line structures. The advantages of using planar components in microwave circuits stem largely from reduced fabrication cost and increased operating bandwidth. Unfortunately, microstrip and coplanar waveguide (CPW) suffer from several problems at millimeter wave frequencies. These include dielectric loss, which increases with frequency, as well as dispersion, substrate moding, and radiation loss, all of which can be directly associated with the air/dielectric discontinuity inherent to substrate supported transmission lines.

Typically, substrate supported structures rely on processing technology such as via holes or substrate thinning to improve millimeter wave performance of planar circuits. An alternate solution to the frequency limitations of conventional planar circuits employs micromachining techniques. This technology, which is widely used in the area of monolithic integrated sensors [1], was first applied to microwave transmission lines in the form of the *microshield line* [2]. This transmission line structure relies on selective silicon etching and membrane supported conductors and can be likened to a CPW line with an air dielectric. Radiation loss into parasitic modes (surface waves) in CPW [3] has been shown to be a function of both f^3 and $(\varepsilon_r - 1)^2$, where f is the frequency and ε_r is the relative dielectric constant of the substrate [4]. Thus, although radiation loss increases rapidly with frequency, it can be eliminated by using an air dielectric. In addition, removal of the silicon substrate eliminates any loss associated directly with the dielectric, and any dispersion related to the dielectric/air interface. Passive microwave circuit components based on microshield line technology have demonstrated excellent performance up to 40 GHz [5]. Recently, a submillimeter wave planar bandpass filter was demonstrated using microshield line [6], and time-domain electro-optic sampling of a CPW line on a membrane has indicated that these lines are capable of propagating signals at frequencies as high as 1000 GHz with low loss and low dispersion [7]. Other planar microwave circuits have employed membrane technology with excellent results. These include a 33 GHz air-microstrip Wilkinson power divider [8] and air-stripline interdigitated bandpass filters at 15 GHz [9]. Micromachining was also applied in the development of a completely shielded CPW line [10].

This paper reports on the application of micromachining technology to *W*-band circuits using the microshield line and a new type of micromachined structure—the shielded membrane microstrip (SMM) line. The fabrication techniques are presented and the design of the *W*-band circuits using a combination of quasi-static and full-wave analysis techniques [10], [11] is discussed. A 90 GHz microshield line low pass filter and several SMM coupled-line bandpass filters centered at 95 GHz are measured. Theoretical validation of the measurements is provided by the finite-difference time-domain (FDTD) analysis technique. This method shows great flexibility and accuracy for *W*-band circuit analysis, and is used to simulate structures which are supported by both GaAs and membrane. Results of these simulations allow for a direct comparison between membrane supported circuits and conventional planar circuits.

II. Membrane Supported Transmission Lines

A. Microshield Line

Microshield line is a nondispersive transmission line which is suspended on a thin dielectric membrane via silicon micromachining techniques in [2], [5], and [12]. The line geometry is best described as a coplanar-waveguide structure situated above a metallized, air-filled cavity (see Fig. 1). Since the microshield line is surrounded entirely by air, its range of possible impedances encompasses higher values than those of substrate supported lines. Typically, microshield lines can be designed to realize characteristic impedances ranging from around 50 Ω to as high as 300 Ω. For filter and other planar circuit applications, it is more logical to work with a higher central impedance than the nominal 50 Ω probe impedance. For this work, characteristic impedances of microshield line have been computed with a conformal mapping method and

Manuscript received June 29, 1995; revised December 18, 1995. This work was supported by NASA and the Office of Naval Research.

The authors are with the Electrical Engineering and Computer Science Department, The University of Michigan, Ann Arbor, MI 48109-2122 USA.

Publisher Item Identifier S 0018-9480(96)02342-3.

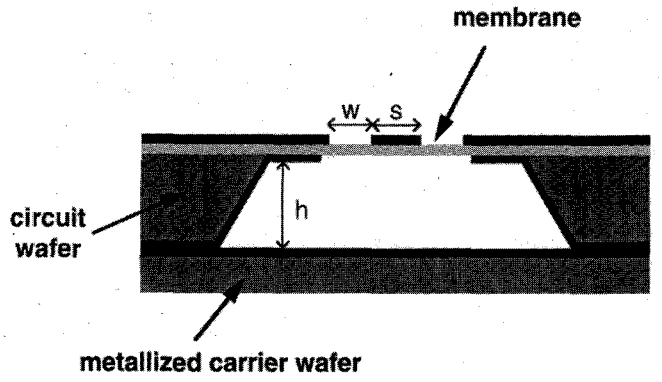

Fig. 1. A two-dimensional representation of the microshield line geometry. The cavity height, h, is determined by the thickness of the wafer, which supports the membrane structure.

with a point-matching method [13]. A value of 92 Ω was selected for the nominal impedance of the line, and this was realized by setting the slot separation, s, to 220 μm, and the slot width, w, to 50 μm for $h = 355\mu$m.

B. Shielded Membrane Microstrip (SMM)

Thin dielectric membranes also provide the foundation for SMM lines. The SMM line is essentially a shielded microstrip line with an air dielectric and also benefits from low dispersion and low dielectric loss. The geometry resembles that of a stripline, but the conducting strip is not positioned symmetrically between the two ground planes. Assembly of the SMM lines requires multiple micromachining steps, including the incorporation of a second micromachined wafer to form a shield. This type of micromachined shielding cavity has been used with completely shielded CPW structures on silicon substrates [10], and with membrane stripline geometries [9]. For SMM, the micromachined cavity actually provides the ground plane for the microstrip signal, and this is accomplished with a three-wafer assembly as illustrated in Fig. 2. The middle circuit wafer rests on a metallized carrier wafer which acts to provide a shielding cover for the microstrip. The ground plane, then, resides *above* the signal line since the micromachined cavity wafer rests on top of the entire structure. The cover height, h_c, is determined by the thickness of the circuit wafer, and the signal-to-ground separation, h, is determined by the etched depth of the micromachined cavity in the ground plane wafer. Impedance calculations for the SMM line can be done easily with two-dimensional (2-D) static methods, but must take into account both metallized shielding surfaces.

III. Fabrication Techniques

The various fabrication techniques used in the micromachining of planar transmission line structures are summarized in [8]–[10], [12], and [14]. These include details of growing the membranes, which are 1.5-μm-thick, three-layer, $SiO_2/Si_3N_4/SiO_2$ dielectric composites, and of the ethylenediamene pyrocatechol (EDP) wet silicon etching process used to micromachine the cavities for different transmission line geometries.

The metal pattern definition and cavity etching are accomplished using standard lithographic processing techniques, but formation of the ground plane cavity requires specific attention. The depth of the cavity must be controlled precisely, since it is crucial in achieving the desired line performance, and this is done by timing the etch. The silicon etch rate for the University of Michigan EDP process [15] has been experimentally determined to be approximately 1.2 μm/min. Rate dependencies on temperature and etch area create difficulties in precise control of the depth of the shielding cavity, but it is believed that an accuracy of $\pm 5\,\mu$m can be obtained. For a nominal cavity depth of 100 μm, FDTD analysis shows that a variation in depth of ±5% will cause less than 1% deviances in center frequency and bandwidth for a 4.3% bandwidth filter centered at 94 GHz. In the future it will be useful to develop etching techniques which are more controllable, but it is important to maintain the smooth surface finish that is achieved with the EDP process, since the etched surface provides an electrical ground plane to the micromachined circuits.

Formation of windows for on-wafer probing access to the circuits can be accomplished by a two-step process which etches the ground plane wafer from both sides and simultaneously forms both the ground plane cavities and the probe windows [10]. The two-step process uses 350-μm-thick, single-side polished silicon wafers with 1.2-μm-thick layers of SiO_2 thermally grown on both sides. It begins with the deposition of a Cr/Au 250/2 000 Å masking layer to define the shielding cavity pattern on the polished (front) side of the wafer. Then, backside alignment is used to define the probe window pattern on the unpolished (back) side of the wafer, and another Cr/Au masking layer is deposited. With the front side protected by photoresist, the back-side oxide is etched in BHF to expose the silicon surface. The wafers are then placed in EDP, and the probe windows are selectively etched from the backside to a depth of 250 μm. The wafers are removed from EDP, cleaned, and placed in BHF, this time removing the front side oxide layer and exposing the silicon on the polished side of the wafer. A final etch in EDP to a depth of 100 μm defines the ground planes for the transmission lines and creates the probing windows which are etched from both sides during the second etch step. The ground plane wafer is subsequently stripped of all masking layers and remetallized with Ti/Al/Ti/Au to a thickness of approximately 1.2 μm. Upon completion of this step, the ground plane wafer is attached to the circuit wafer such that the etched windows permit access to the GCPW probe pads, and this two-wafer assembly is then placed on a metallized carrier wafer to complete the circuit enclosure.

IV. *W*-Band Circuit Development

Generally, *W*-band circuit development requires the use of both quasi-static and full-wave analysis techniques due to parasitics which affect circuit performance much more severely at *W*-band than at lower frequencies [10], [11]. In addition, experimental low-frequency modeling can be used to provide additional insight into *W*-band planar circuit performance [14].

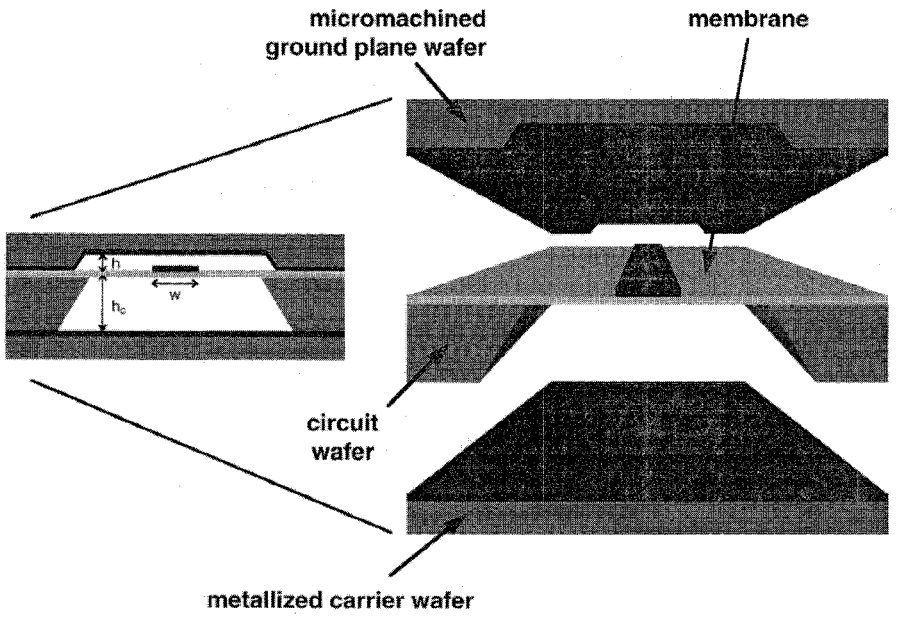

Fig. 2. Geometry of SMM. This membrane supported transmission line requires micromachining of two separate wafers which are subsequently assembled to form the final structure.

A. Grounded-CPW to SMM Transition

For on-wafer probing of SMM line structures, consideration must be given to the manner in which the grounded-CPW (GCPW) geometry of the probe pad can be transformed to provide a field distribution compatible with the SMM line. The propagating mode of the SMM line is characterized by an electric field orientation which is primarily vertical with respect to the plane of the signal line. Conversely, a horizontally opposed electric field orientation prevails in a CPW-style wafer probe. One possible candidate for a transition between these two modes is the microshield line, which has shown the ability to support both CPW-like and a microstrip-like modes [12]. The ratio of slot width to ground plane height determines whether a microstrip mode or a CPW mode is excited on the line. When the slot width is large compared to the ground plane height, the propagating electric fields tend to concentrate under the center conductor of the structure with a vertical orientation which is very similar to the dominant mode of microstrip propagation. Conversely, when the slots are narrow with respect to the ground plane height, the electric fields adopt a horizontally opposed orientation which is characteristic of the odd mode in CPW lines. This is exemplified in Fig. 3 by the plot of the microshield line characteristic impedance versus normalized slot width. For smaller w/h ratios, the impedance is very sensitive to changes in the slot width, indicating a strong horizontal component in the electric field and a CPW-like mode of propagation. As w/h increases, however, the dependence on the slot width decreases, and the impedance gradually approaches that of a microstrip line with the same s/h ratio.

A tapered section of microshield line, then, could be used to implement an effective transition between the two different modes of the CPW wafer probe and the SMM line. This is a very convenient solution, since there is an impedance mismatch between the 50 Ω wafer probe and the 92 Ω SMM line, and a tapered section of microshield line can also be used to accomplish the impedance matching function. Fig. 3 provides design data for a Klopfenstein impedance matching taper, which is an approximation to a Chebyshev matching transformer of infinite order [16], [17]. A schematic of the taper is shown in Fig. 4, including the CPW probe pad and the SMM line. The taper is designed so that the width of the microshield center conductor remains constant, while the slot widths gradually increase. At each end of the taper, the geometry of the microshield line provides a field distribution that is compatible with the appropriate type of transmission line.

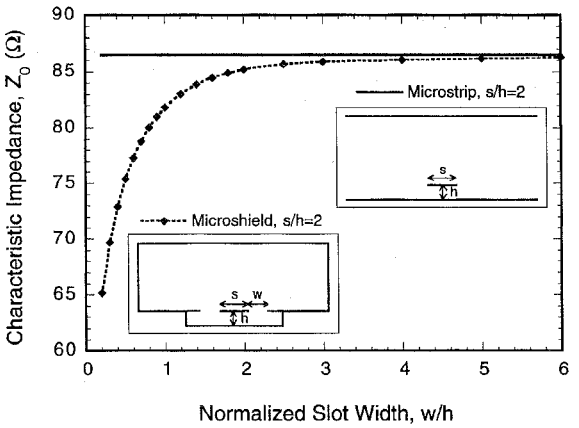

Fig. 3. Impedance of a microshield line with an upper shield, calculated using the point-matching method. The solid line indicates the asymptotic limit for the line impedance, which is represented by the impedance of a microstrip line (calculated quasi-statically) with an equivalent s/h ratio.

B. Low Pass Filters

A low pass filter designed using a stepped impedance implementation of a seven-section 0.5 dB equal ripple Cheby-

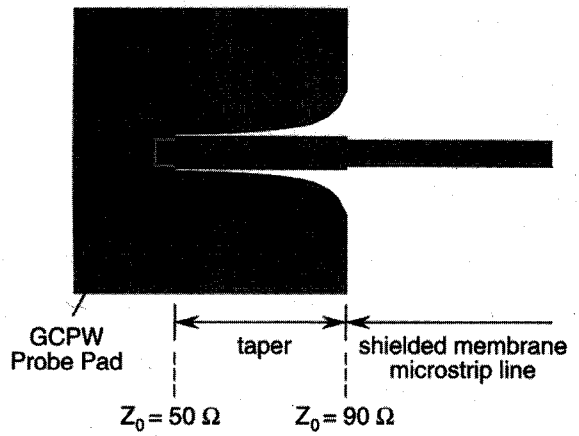

Fig. 4. Layout of the Klopfenstein taper used as a transition from the GCPW probe pad to SMM line. The entire circuit is supported on the thin dielectric membrane, with the exception of the probing areas, which are located on the silicon support rim at the edge of the membrane area.

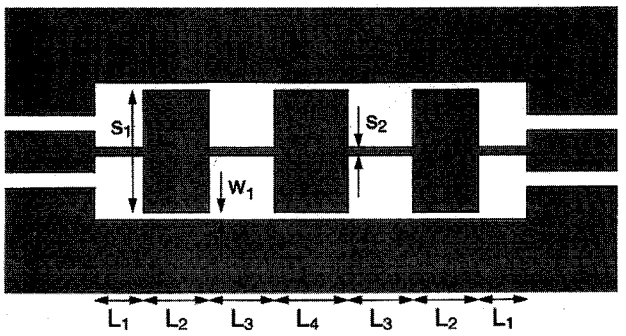

Filter Type	s_1	w_1	s_2	L_1	L_2	L_3	L_4
Microshield Line	540	20	20	220	340	360	420
GCPW on GaAs	230	20	10	120	80	200	80

Fig. 5. Layout of the stepped-impedance low pass filter. Dimensions (in μm) for microshield line and GCPW on GaAs configurations are given in the table.

shev filter prototype is shown in Fig. 5 [18]. The high and low impedance sections of the filter correspond to 277 Ω and 63 Ω, respectively, while the feed line and filter center impedance are designed to be 92 Ω. The filter section lengths were initially approximated by means of equivalent circuit models for short transmission line sections. Then, quasi-static simulation on *Puff* [19] was used to adjust the stage lengths more accurately. The final step in the design sequence involved full-wave analysis of the filter using the FDTD method. The first FDTD simulation revealed that the filter cutoff frequency was lower than the desired 90 GHz value, so the filter section lengths were scaled appropriately to achieve the correct cutoff frequency.

C. Bandpass Filters

The bandpass filters of this work are based on coupled-line resonator designs derived from equal ripple Chebyshev prototypes [20]. Both three- and five-element filters of various bandwidths were designed based on a center impedance of 90 Ω [21]. A commercially available software package, PARFIL [22], was used to synthesize the filter geometry,

TABLE I
DIMENSIONS OF THE COUPLED-LINE SECTIONS IN THE BANDPASS FILTERS

Filter Section Index, k	6% Bandwidth Filter	
	width (w_k)	separation (s_k)
$k = 1,6$	160 μm	70 μm
$k = 2,5$	180 μm	270 μm
$k = 3,4$	180 μm	300 μm
Filter Section Index, k	**13% Bandwidth Filter**	
	width (w_k)	**separation (s_k)**
$k = 1,6$	140 μm	30 μm
$k = 2,5$	180 μm	140 μm
$k = 3,4$	180 μm	180 μm
Filter Section Index, k	**18% Bandwidth Filter**	
	width (w_k)	**separation (s_k)**
$k = 1,4$	155 μm	25 μm
$k = 2,3$	180 μm	105 μm

using a ground plane separation and an upper shield separation of 100 μm and 500 μm, respectively. The PARFIL designs were verified by constructing a 2 GHz 47:1 scale model of a 4.3% bandwidth five-element filter. The dielectric membrane was simulated by a 76-μm-thick polyethylene sheet and the filter metallization patterns were defined using copper tape. Measurements of the 2 GHz filter revealed that the filter center frequency was not accurately predicted by PARFIL, but the measured bandwidth agreed well with the PARFIL data. The PARFIL design values for line widths and gap spacings were therefore used in the *W*-band implementation, but the resonator lengths were determined through experimental iteration on the low-frequency model (for dimensions, see Table I in Section V). The desired filter center frequency was achieved when the resonator lengths were scaled to 94.7% of the original design lengths (710 μm instead of 750 μm), and this was confirmed with FDTD simulations at 94 GHz. The effect of the upper shielding cavity was also investigated using the microwave model, and the measured response of the filter changed significantly when the upper shielding surface was removed. Fig. 6 shows that the low-frequency corner of the bandpass response became severely degraded due to radiation losses in the case of the open structure.

V. *W*-Band Measurements and Discussion

W-band measurements were performed on an HP 8510C Vector Network Analyzer with an HP 85105A millimeter wave controller [23]. On-wafer probing was achieved on a probe station using Model 120 Picoprobes with 150 μm pitch [24]. The DEEMBED calibration program from NIST [25] provided an automated calibration routine based on the

TABLE II
LOADED QUALITY FACTORS (Q_L'S) OF SMM RESONATORS

Filter Bandwidth	Measured S_{21}	Estimated Mismatch Loss	Resonator Q_L
6.1%	3.6 dB	0.6 dB	199
12.5%	2.2 dB	0.6 dB	155
17.7%	1.4 dB	0.6 dB	155

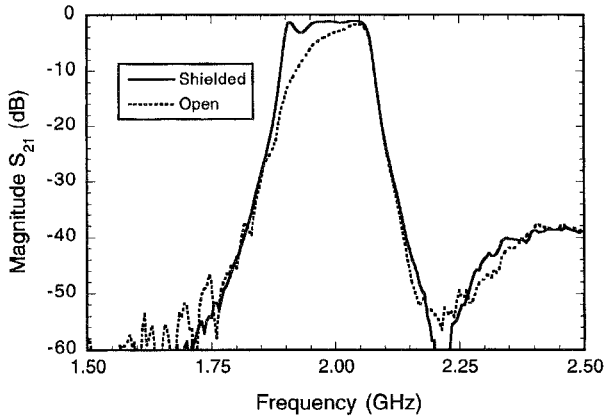

Fig. 6. Measurements of a 47:1 scale model of a SMM bandpass filter. Comparison between shielded and open geometries shows the detrimental performance of the open case caused by radiation losses in the filter.

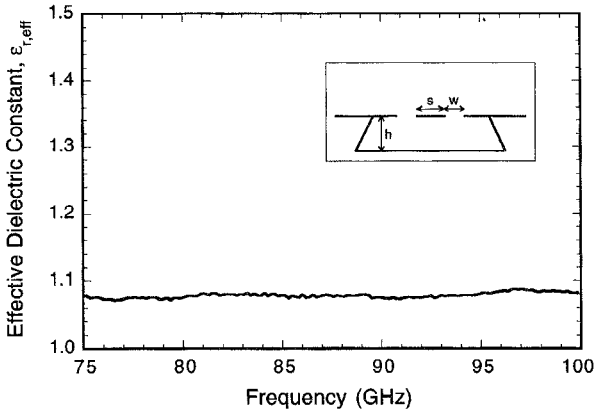

Fig. 7. Measured effective dielectric constant of a microshield line. Dimensions in μm are: $s = 220$, $w = 45$, $h = 355$. Data obtained using the NIST program DEEMBED.

thru-reflect-line (TRL) technique [26], [27]. The calibration standards comprised a series of uniform transmission lines (thru and line types) and either an open- or short-circuited transmission line to provide the "reflect." They were fabricated in conjunction with the filter circuits to minimize differences between the standards and the circuits of interest due to processing variations.

Since membranes are not strong enough to withstand the pressure of repeated on-wafer probing, wafer probes must be placed on the silicon support rim of the membrane structure. For *W*-band measurements, it was found that the best results were achieved when the wafer probes were set as close as possible to the membrane edge. Furthermore, an impedance transformer was used to reduce the matching problems between the high-impedance membrane circuits and the 50 Ω test system impedance. For 92 Ω microshield line, this took the form of a simple quarter-wavelength section of 68 Ω microshield line. For the SMM filters, the previously described GCPW-to-SMM transition was employed.

The deembedding software also calculates the effective relative dielectric constant ($\varepsilon_{r,\text{eff}}$) of the transmission line [28] (Fig. 7). The measured value of $\varepsilon_{r,\text{eff}} = 1.08$ for the microshield line is due to the presence of the three-layer $SiO_2/Si_3N_4/SiO_2$ membrane, whose constituent layers have dielectric constant values of approximately 4.0/7.5/4.0, respectively. It is noted that the measured value of $\varepsilon_{r,\text{eff}}$ is highly dependent on the microshield line geometry, since lines with different $s/(s + 2w)$ ratios will produce different levels of field concentration within the membrane [5]. The measured $\varepsilon_{r,\text{eff}}$ remains constant from 75–100 GHz, showing that the membrane causes very little dispersion. Calibration data from the SMM standards was not as smooth as for the microshield lines, but it shows the same properties of low loss and low dispersion. The measured $\varepsilon_{r,\text{eff}}$ for the SMM lines is approximately 1.04.

A. Low Pass Filters

The measured response of the low pass filter from 75–110 GHz is plotted in Fig. 8 along with results of the FDTD analysis from 40–140 GHz. The filter achieves a cutoff frequency of approximately 90 GHz, with less than 1 dB passband insertion loss, and the FDTD technique accurately predicts the filter performance. The presence of the membrane does not have a negligible effect on the performance of the circuit, and it is therefore incorporated into the FDTD analysis. It is not exactly modeled as a 1.5-μm-thick dielectric sheet, however, since the mesh subsection size in the vertical direction is 44 μm. Instead, a sheet of dielectric with a thickness of 44 μm is placed underneath the conducting lines of the structure. The relative dielectric constant of this "thick membrane" is set to 1.16, so that the effective dielectric constant predicted by the FDTD analysis corresponds to the measured value of 1.08. This method of compensation only provides an approximate model of the membrane effects, however, because the measured $\varepsilon_{r,\text{eff}}$ strongly depends on line geometry. Different line geometries will require individually designed "thick membranes" for accurate FDTD simulations.

An FDTD analysis was also performed for an equivalent low pass filter designed using grounded-CPW (GCPW) on a 100-μm GaAs substrate ($\varepsilon_r = 12.7$). This filter was synthesized using the same Chebyshev prototype values and short transmission line models as used in the design of the

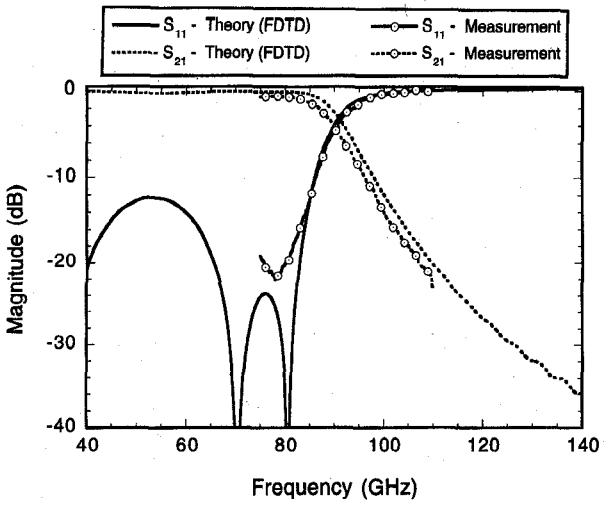

Fig. 8. Measured and predicted performance of a 90-GHz microshield low pass filter.

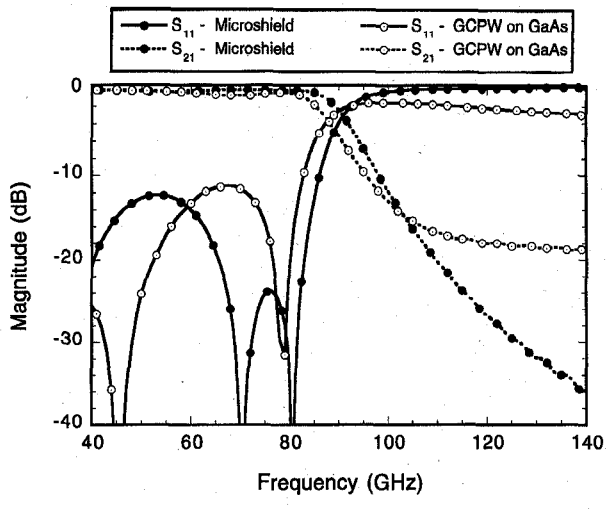

(a)

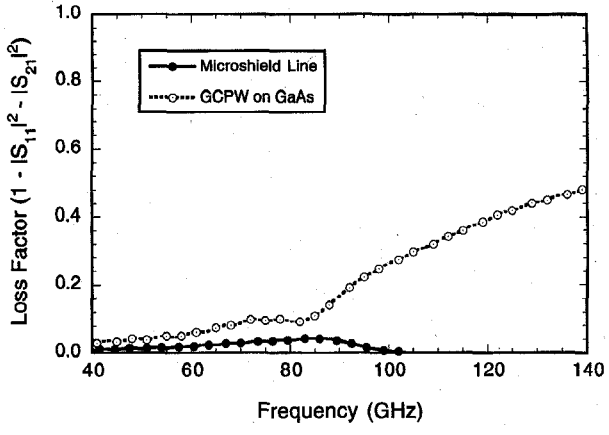

(b)

Fig. 9. (a) Theoretical performance of a low pass filter fabricated using both microshield line and GCPW on GaAs. (b) Comparison of theoretical radiation losses in a low pass filter realized in microshield line and in GCPW on GaAs. Above 100 GHz the data for the microshield filter becomes negative due to numerical error in the FDTD simulation.

microshield line filter, and impedances for the GCPW lines were found from a conformal mapping method calculation [29]. FDTD simulations were performed to scale the filter response to the desired 90 GHz cutoff frequency, but no further design optimizations were attempted. The microshield line filter provides 20 dB more out-of-band attenuation than the GCPW filter, and the return loss of the GCPW filter degrades with increasing frequency, while the microshield filter return loss remains high [see Fig. 9(a)]. The graph in Fig. 9(b) explains that the poor performance of the GCPW filter above the cutoff frequency can be attributed to increased radiation losses. The calculated loss factors shown in this plot do not include conductor or dielectric losses. It should be noted that while it is possible to improve the performance of the GCPW filter on GaAs, this requires extensive design iteration that was not performed for the purposes of this comparison. The GCPW filter shown here demonstrates the typical problems encountered when using traditional dielectric substrates such as GaAs.

B. Bandpass Filters

Fig. 10 shows a fabricated coupled-line bandpass filter. Three such filters were tested, and the measured results for all of them show low passband insertion loss, sharp roll-off, and high out-of-band attenuation. A filter designed for 4.25% bandwidth (pictured in Fig. 10) achieves a passband insertion loss of 3.6 dB and a bandwidth of 6.1% at a center frequency of 94.7 GHz (see Fig. 11). Fig. 12 shows the response of a five-element filter designed for 8.5% bandwidth with a measured insertion loss of 2.2 dB and a 12.5% bandwidth centered at 95 GHz. Measurements of a three-element, 12.8% bandwidth filter are shown in Fig. 13. This filter has a measured insertion loss of 1.4 dB, a center frequency of 94.9 GHz, and a bandwidth of 17.7%. Dimensions of these filters are listed in Table I.

Measured S-parameters of the three bandpass filters reveal wider bandwidths than the designed values, due to the manner in which the SMM circuits were assembled. The attachment

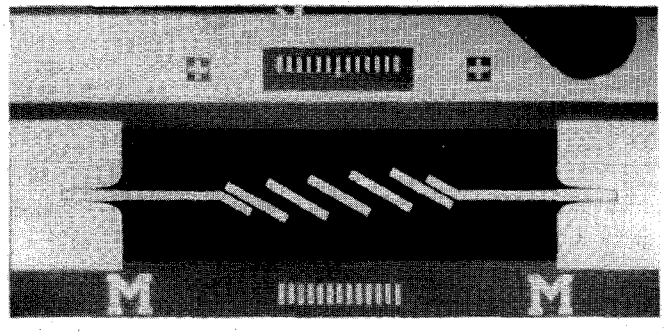

Fig. 10. Photograph of a five-section bandpass filter in SMM. The ground plane cavity wafer has been removed for viewing, and the membrane portions of the circuit are visible as darkened regions compared to the lighter gray silicon support rim.

of the lower ground cavity wafer was accomplished with small beads of photoresist "glue," which possessed nonzero thicknesses. As a result, the distance from the signal line to the ground plane was approximately 20 μm longer than the 100 μm depth of the ground cavity. This is verified by the

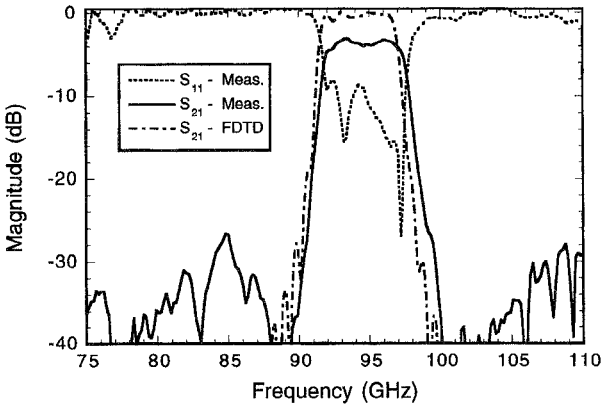

Fig. 11 Measured S-parameters of a five-section SMM coupled line bandpass filter with 3.4 dB insertion loss and 6.1% bandwidth at 94.7 GHz. The FDTD analysis shown uses a 15-μm-thick dielectric sheet with $\varepsilon_r = 1.1$ to model the effects of the thin membrane.

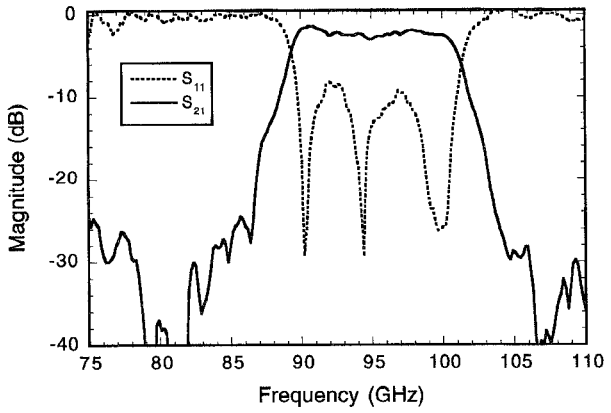

Fig. 12. Measured S-parameters of a five-section SMM coupled line bandpass filter with 2.2 dB insertion loss and 12.5% bandwidth at 95 GHz.

TABLE III
DIMENSIONS OF THE COUPLED-LINE SECTIONS IN THE BANDPASS FILTERS ON GaAs

Filter Section Index, k	width (w_k)	separation (s_k)
$k = 1,6$	70 μm	70 μm
$k = 2,5$	80 μm	190 μm
$k = 3,4$	80 μm	220 μm

good agreement with the FDTD analysis shown in Fig. 11, which was performed using a ground plane separation of 120 μm. For this analysis, a "thick membrane" with a thickness of 15 μm and a dielectric constant of 1.1 was used to simulate the effects of the 1.5 μm dielectric membrane (again, the relative dielectric constant of the thick membrane was chosen to give close agreement between measured and FDTD values of $\varepsilon_{r,\text{eff}}$).

The losses in the measured filter responses are assumed to be entirely due to conductor losses within the filter, as has been proven for air-stripline resonators [30]. This is verified by PARFIL analysis, which predicts a passband insertion loss of 3.4 dB for the narrow-band (6.1%) filter when only conductor losses are included (metallization is 4000 Å Au). The losses are

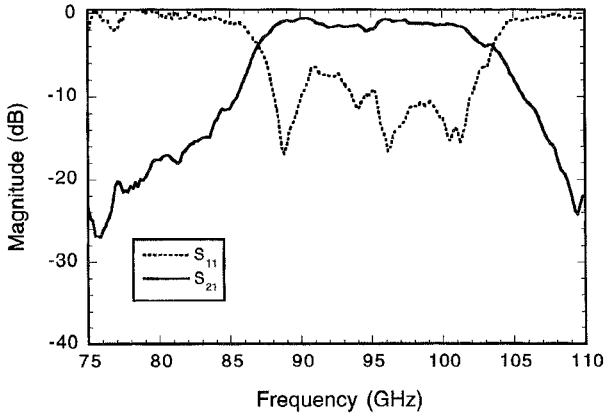

Fig. 13. Measured S-parameters of a three-section SMM coupled line bandpass filter with 1.4 dB insertion loss and 17.7% bandwidth at 94.9 GHz.

also used to extract values for the loaded Q's of the resonators in each of the filters. This is done assuming the filters consist of uniform resonators according to the method presented in [20]. Table II summarizes the values found for the loaded Q's of the resonators in each filter.

As with the low pass filter, the FDTD analysis was used to compare the performance of an SMM bandpass filter to an equivalent coupled line bandpass filter realized on GaAs. Once again, a very simple design methodology was performed to realize the filter on GaAs; the filter dimensions were synthesized using PARFIL, and the resonator lengths were scaled to 230 μm based on FDTD simulations. The ground plane separation was 100 μm and the cover height was 500 μm, but the substrate dielectric constant was 13 instead of 1. For the purposes of comparison, no effort was made to compensate for the effects of the dielectric substrate (e.g., via holes or waveguide enclosures). The dimensions of the filter on GaAs are provided in Table III for comparison to the SMM filter dimensions. The theoretical performance of the filter on GaAs is plotted in Fig. 14(a), and a severe degradation in performance is observed in comparison with the membrane supported circuit. The filter pass band is nonsymmetric and the out-of-band signal rejection suffers due to radiation losses. Fig. 14(b) shows the high levels of substrate radiation which plague the filter—note that nearly half of the input power is lost to radiation around the low frequency corner of the filter response. Specialized fabrication techniques can be used to alleviate these problems, but they usually result in increased circuit complexity and cost.

VI. CONCLUSION

This paper presents a study of membrane supported micromachined transmission lines for applications in W-band frequencies (75–110 GHz). Both low pass and bandpass filters are discussed, as well as issues pertaining to on-wafer probing and transitions to membrane supported lines. Measured circuit performance is very good and demonstrates the ability of micromachined transmission lines to provide very high performance planar circuits at millimeter wave frequencies. Also demonstrated is the ability of the finite-difference time-domain technique to provide accurate simulation of measured circuit

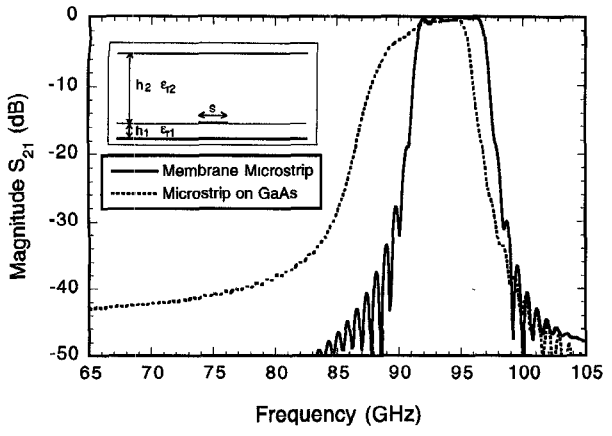

(a)

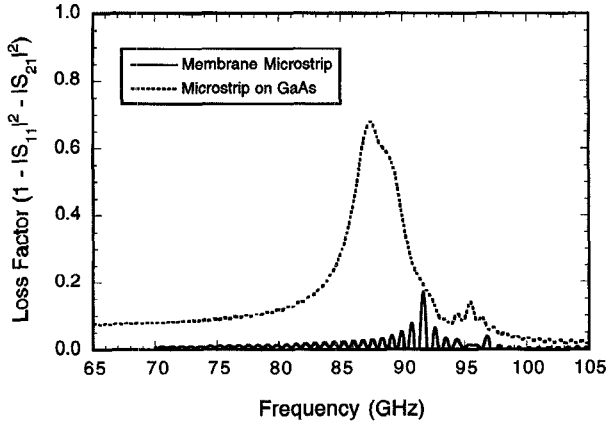

(b)

Fig. 14. (a) Theoretical performance of a coupled line bandpass filter using both conventional microstrip (on GaAs) and SMM. Results are from the FDTD analysis. (b) Modeled radiation losses in the bandpass filter in both conventional microstrip and SMM line. Loss factors are calculated from the results of FDTD simulations.

responses. The FDTD also provided a tool for comparison to substrate-supported circuits. These comparisons showed that the parasitic effects of radiation and dispersion can severely degrade performance in conventional planar circuits unless they are reduced or eliminated through extensive design and fabrication procedures. Micromachining and membrane technology provide an option for effectively eliminating dispersion, radiation loss, and dielectric loss in high performance, millimeter-wave, planar circuits.

ACKNOWLEDGMENT

The authors would like to thank Prof. R. F. Drayton of the University of Illinois-Chicago, formerly of the University of Michigan, and Prof. T. M. Weller of the University of South Florida, formerly of the University of Michigan, for their discussions concerning circuit fabrication. Also, Dr. N. I. Dib of Jordan University of Science and Technology, formerly of the University of Michigan, for supplying the FDTD code, and G. E. Ponchak of NASA-Lewis/University of Michigan for use of the *W*-band probe station and his assistance with the measurements.

REFERENCES

[1] R. S. Muller, *et al*, Eds., *Microsensors*. New York: IEEE Press, 1991.
[2] N. I. Dib, W. P. Harokopus, L P. B. Katehi, C. C. Ling, and G. M. Rebeiz, "Study of a novel planar transmission line," in *1991 IEEE MTT-S Dig.*, pp. 623–626.
[3] R. W. Jackson, "Considerations in the use of coplanar waveguide for millimeter-wave integrated circuits," *IEEE Trans. Microwave Theory Tech.*, vol. MTT-34, no. 12, pp. 1450–1456, Dec. 1986.
[4] R. Y. Yu, M. Reddy, J. Pusl, S. T. Allen, M. Case, and M. J. W. Rodwell, "Millimeter-wave on-wafer waveform and network measurements using active probes," *IEEE Trans. Microwave Theory Tech.*, vol. 43, no. 4, Apr. 1995.
[5] T. M. Weller, L. P. B. Katehi, and G. M. Rebeiz, "High performance microshield line components," *IEEE Trans. Microwave Theory Tech.*, vol. 43, no. 3, pp. 534–543, Mar. 1995.
[6] ——, "A 250 GHz microshield bandpass filter," *IEEE Microwave and Guided Wave Lett.*, vol. 5, no. 5, May 1995.
[7] H. J. Cheng, J. F. Whitaker, T. M. Weller, and L. P. B. Katehi, "Terahertz-bandwidth characterization of coplanar waveguide on dielectric membrane via time-domain electro-optic sampling," in *1994 IEEE MTT-S IMS Dig.*, pp. 477–480.
[8] T. M. Weller, L. P. B. Katehi, M. I. Herman, and P. D. Wamhof, "Membrane technology (MIST-T) applied to microstrip: A 33 GHz Wilkinson power divider," in *1994 IEEE MTT-S Dig.*, pp. 911–914.
[9] C.-Y. Chi and G. M. Rebeiz, "Planar microwave and millimeter-wave lumped elements and coupled-line filters using micro-machining techniques," *IEEE Trans. Microwave Theory Tech.*, vol. 43, no. 4, pp. 730–738, Apr. 1995.
[10] R. F. Drayton and L. P. B. Katehi, "Development of self-packaged high frequency circuits using micromachining techniques," *IEEE Trans. Microwave Theory Tech.*, vol. 43, no. 9, pp. 2073–2080, Sept. 95
[11] H. Wang, *et al*, "High-performance *W*-band monolithic pseudomorphic InGaAs HEMT LNA's and design/analysis methodology," *IEEE Trans. Microwave Theory Tech.*, vol. 40, no. 3, pp. 417–426, Mar. 1992.
[12] T. M. Weller, G. M. Rebeiz, and L. P. B. Katehi, "Experimental results on microshield transmission line circuits," in *1993 IEEE MTT-S Dig.*, pp. 827–830.
[13] N. I. Dib and L. P. B. Katehi, "Impedance calculation for the microshield line," *IEEE Microwave Guided Wave Lett.*, vol. 2, no. 10, pp. 406–408, Oct. 1992.
[14] C. Y. Chi and G. M. Rebeiz, "A low-loss 20 GHz micromachined bandpass filter," in *1995 IEEE MTT-S Dig.*, pp. 1531–1534.
[15] T. M. Weller, "Micromachined high frequency transmission lines on thin dielectric membranes," Ph.D. dissertation, Univ. of Michigan, pp. 200–204, 1995.
[16] R. W. Klopfenstein, "A transmission line taper of improved design," *Proc. IRE*, vol. 44, pp. 31–35, Jan. 1956.
[17] M. A. Grossberg, "Extremely rapid computation of the Klopfenstein impedance taper," *Proc. IEEE*, vol. 56, pp. 1629–1630, Sept. 1968.
[18] S. V. Robertson, L. P. B. Katehi and G. M. Rebeiz, "*W*-band microshield low pass filters," in *1994 IEEE MTT-S Dig.*, pp. 635–628.
[19] S. W. Wedge, R. Compton, and D. Rutledge, *Puff: Computer Aided Design for Microwave Integrated Circuits*, ver. 2.0, copyright 1991, Puff Distribution, Electrical Engineering M/S 116-81, California Institute of Technology, Pasadena, CA 91125.
[20] G. Matthaei, L. Young, and E. M. T. Jones, *Microwave Filters, Impedance-Matching Networks, and Coupling Structures*. Norwood, MA: Artech House, 1980, pp. 100–101 and 149–153
[21] S. V. Robertson, L. P. B. Katehi, and G. M. Rebeiz, "Micromachined self-packaged *W*-band bandpass filters," in *1995 IEEE MTT-S Dig.*, pp. 1543–1546.
[22] WaveCon Software, El Segundo, CA.
[23] Hewlett-Packard Company, Santa Clara, CA.
[24] GGB Industries, Inc., Naples, FL.
[25] R. B. Marks and D. F. Williams, NIST De-embedding Software, Program DEEMBED, Revision 4.04.
[26] G. F. Engen and C. A. Hoer, "Thru-reflect-line: An improved technique for calibrating the dual six-port automatic network analyzer," *IEEE Trans. Microwave Theory Tech.*, vol. MTT-27, no. 12, pp. 897–993, Dec. 1979.
[27] R. B. Marks, "A multiline method of network analyzer calibration," *IEEE Trans. Microwave Theory Tech.*, vol. 39, no. 7, pp. 1205–1215, July 1991.
[28] D. F. Williams and R. B. Marks, "Transmission line capacitance measurement," *IEEE Microwave Guided Wave Lett.*, vol. 1, no. 9, pp. 243–245, Sept. 1991.
[29] C. Veyres and V. F. Hanna, "Extension of the application of conformal mapping techniques to coplanar lines with finite dimensions," *Int. J.*

Electronics, vol. 48, no. 1, pp. 47–56, 1980.
[30] C-Y. Chi and G. M. Rebeiz, "Conductor-loss limited stripline resonators and filters," submitted to *IEEE Trans. Microwave Theory Tech.*, June 1995.

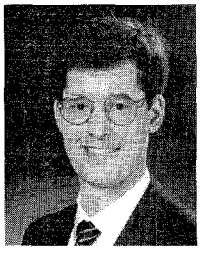

Stephen V. Robertson, (S'93) received the B.S.E.E. degree from the University of Texas, Austin, TX, and the M.S.E. degree from the University of Michigan, Ann Arbor, MI, in 1991 and 1993, respectively. He is currently pursuing the Ph.D. degree in electrical engineering at the University of Michigan.

His research interests lie in the development of novel micromachined structures for planar and quasi-planar millimeter-wave applications.

Linda P. B. Katehi (S'81–M'84–SM'89–F'95), for a photograph and biography, see p. 3 of the January 1996 issue of this TRANSACTIONS.

Gabriel M. Rebeiz (S'86–M'88–SM'93), received the Ph.D. degree in electrical engineering from the California Institute of Technology, in June 1988.

He joined the faculty of the University of Michigan in 1988 and was promoted to Associate Professor in 1992. He was a Visiting Professor at Chalmers University of Technology in 1992, and a Visiting Professor at the Ecole Normale Superieur in 1993. He is the author of 62 papers published in refereed journals and more than 110 papers presented at national and international conferences. His interests are in applying micromachining techniques in silicon and GaAs for the development of low-loss and low-cost microwave antennas, components and subsystems for wireless applications and satellite communication systems. He is also interested in the development of mm-wave high-efficiency antennas, planar collision-avoidance sensors for automotive applications, and in millimeter-wave imaging and phased arrays, and in monopulse tracking systems.

Dr. Rebeiz received the National Science Foundation Presidential Young Investigator Award in 1991 and the URSI International Isaac Koga Gold Medal Award for Outstanding International Research in 1993. He also received the Research Excellence Award in 1995 from the University of Michigan. Together with his students, he is the winner of best paper awards at JINA '90, IEEE-MTT '92, '94, '95 and IEEE-AP '92 and '95. He is an elected member of URSI-D.